Activation and control of p53 tetramerization in individual living cells

Giorgio Gaglia[a], Yinghua Guan[a,b], Jagesh V. Shah[a,b,1], and Galit Lahav[a,1]

[a]Department of Systems Biology, Harvard Medical School, Boston, MA 02115; and [b]Renal Division, Brigham and Women's Hospital, Boston, MA 02115

Edited by Alan R. Fersht, Medical Research Council Laboratory of Molecular Biology, Cambridge, United Kingdom, and approved August 9, 2013 (received for review June 11, 2013)

Homo-oligomerization is found in many biological systems and has been extensively studied in vitro. However, our ability to quantify and understand oligomerization processes in cells is still limited. We used fluorescence correlation spectroscopy and mathematical modeling to measure the dynamics of the tetramers formed by the tumor suppressor protein p53 in single living cells. Previous in vitro studies suggested that in basal conditions all p53 molecules are bound in dimers. We found that in resting cells p53 is present in a mix of oligomeric states with a large cell-to-cell variation. After DNA damage, p53 molecules in all cells rapidly assemble into tetramers before p53 protein levels increase. We developed a model to understand the connection between p53 accumulation and tetramerization. We found that the rapid increase in p53 tetramers requires a combination of active tetramerization and protein stabilization, however tetramerization alone is sufficient to activate p53 transcriptional targets. This suggests triggering tetramerization as a mechanism for activating the p53 pathway in cancer cells. Many other transcription factors homo-oligomerize, and our approach provides a unique way for probing the dynamics and functional consequences of oligomerization.

systems biology | FCS | mathematical model

Homo-oligomerization, the formation of a protein complex out of identical components, is extremely common in nature; in *Escherichia coli* it is estimated that 35% of proteins form homo-oligomers (1), with an average of four subunits per complex. In yeast and human cells many transcription factors undergo homo-oligomerization, which has been shown to be crucial for their function (2). The molecular dynamics of oligomerization have been studied for some proteins in vitro, but no study has quantified a discrete number of oligomers in a dynamic oligomerization process in live single cells. Here we focus on the homo-tetramers formed by the tumor suppressor p53 and quantify the fraction, dynamics, and function of homo-oligomers in single living cells in response to DNA damage.

p53 is a stress-response transcription factor that orchestrates cell fate decisions such as cell-cycle arrest, senescence, and apoptosis. Tetramerization of p53 is required for its direct binding to DNA (3, 4). Mutations in the p53 tetramerization domain (326–356 aa) lead to a reduction in, or loss of, its transcriptional activity in cells (5) and were shown to cause early cancer onset, known as Li–Fraumeni syndrome (6, 7).

In in vitro studies, p53 first assembles into homo-dimers with a K_d of ∼1 nM (8), and these dimers then come together in tetramers with a K_d of ∼100 nM–1 μM (8–11). The K_d of tetramerization in vitro can be lowered by specific posttranslational modifications (10–12). Based on these measurements and the estimated p53 concentration in cells of 140 nM (13), it has been proposed that p53 should be primarily dimeric in basal conditions and that it forms tetramers in stressed conditions (14). However, there is currently no direct experimental evidence for this in cells.

We used fluorescence correlation spectroscopy (FCS) to quantify the fraction of p53 monomers, dimers, and tetramers in living single cells in a basal state and post-DNA damage. FCS is widely used in vitro to measure protein homo-oligomerization, including p53 tetramerization (4, 8), but has only rarely been used in living cells for this purpose (15). FCS provides direct measurements of the intensity and brightness of fluorescent molecules (16); the intensity reports the numbers of fluorescent molecules in the volume and therefore provides a measure of total protein concentration. The brightness captures the average fluorescent intensity of p53 aggregates; hence, higher brightness indicates a higher oligomerization state (Fig. 1*A*). Note that the brightness captures only the interactions between fluorescently labeled molecules, and hence it is not affected by non–homo-oligomeric binding interactions, even when these might affect the diffusion rate (*Materials and Methods*).

Results

p53 Is Present in a Mixture of Oligomeric States in Cells. For FCS to provide an accurate measure of p53 oligomerization state, all p53 molecules must be fluorescently labeled. We therefore established a cell line silenced for endogenous p53 (17) to which we reintroduced an exogenous p53 tagged with mCerulean, a monomeric version of CFP (Fig. S1*A*). Fluorescently tagged p53 was previously shown to mimic the dynamics of endogenous p53 in response to DNA damage (18), and here we show that its function as a transcription factor is analogous to wild-type p53 (Fig. S1*B*). We also constructed cell lines expressing two p53 mutants, which have been extensively tested in vitro: p53 L344A, a mutant that cannot form tetramers but does form dimers, and p53 L344P, a mutant that cannot form dimers or tetramers and is therefore only monomeric (Fig. 1*B*).

Significance

p53 oligomerization has been the topic of many previous studies, mainly due to the connection between mutations in the p53 tetramerization domain and Li–Fraumeni syndrome. However, all previous studies have measured p53 oligomeric state in vitro. We measure the dynamics of p53 oligomerization in living cells using fluorescence correlation spectroscopy and quantify the discrete number of oligomers over time after DNA damage. Our study demonstrates the power of using sensitive analytical tools for acquiring accurate measures of fluctuation correlation in living cells and the use of mathematical models to gain new insights about p53 biology. The approach we used here should be of general utility in studying the quantitative dynamics and function of protein oligomerization in any cellular system.

Author contributions: G.G., J.V.S., and G.L. designed research; G.G. and Y.G. performed research; Y.G. contributed new reagents/analytic tools; G.G. and Y.G. analyzed data; and G.G., J.V.S., and G.L. wrote the paper.

The authors declare no conflict of interest.

This article is a PNAS Direct Submission.

[1]To whom correspondence may be addressed. E-mail: jagesh@hms.harvard.edu or galit@hms.harvard.edu.

This article contains supporting information online at www.pnas.org/lookup/suppl/doi:10.1073/pnas.1311126110/-/DCSupplemental.

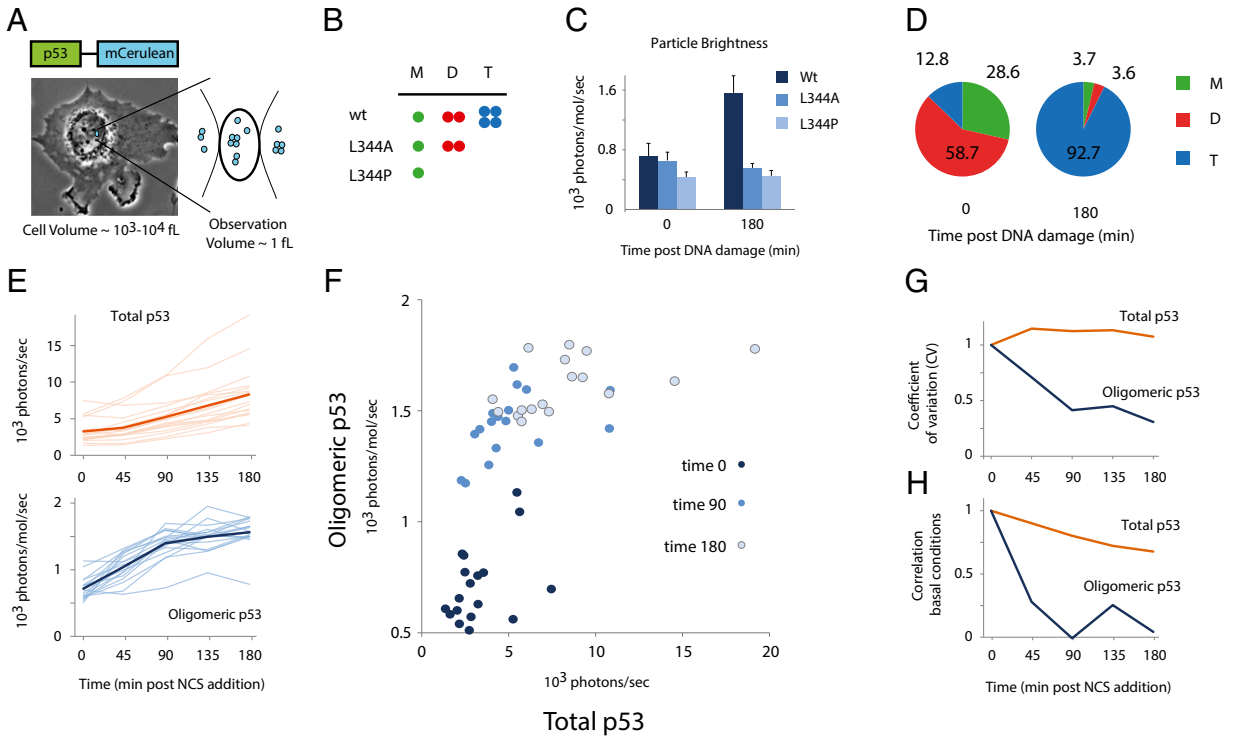

Fig. 1. The dynamics of p53 oligomerization in cells can be studied using FCS. (*A* and *B*) Schematic view of FCS measurement. The FCS measurements were obtained with a two-photon excitation laser in the nucleus of live cells. The laser creates an observation volume of ~1 fL, through which fluorescently labeled p53 molecules diffuse. (*B*) Wild-type p53 forms dimers (D) and tetramers (T). Mutant p53 L344A forms dimers but no tetramers, and p53 L344P mutant is only monomeric (M). (*C*) p53 oligomerization is induced after DNA damage. The oligomerization state is represented by the particle brightness. (*D*) Percentages of p53 monomers, dimers, and tetramers in basal conditions (*Left*) and after DNA damage (*Right*). (*E* and *F*) Dynamics of total and oligomeric p53 post-DNA damage. Each trajectory in *E* is a single cell. The bold line is the average behavior. Each dot in *F* is one single-cell measurement at the indicated time after DNA damage. Note that in the first 90 min after DNA damage, cells mainly move vertically in the scatter plot, indicating that oligomerization increases, whereas total p53 does not change. In the following 90 min (180 min post damage) cells mostly move horizontally, indicating that now the concentration of p53 increases with a minimal change in the oligomerization state. (*G*) Cell-to-cell variation of total and oligomeric p53. Note that the coefficient of variation (CV) for total p53 does not change post damage, meaning that the variation between cells is constant. In contrast, the CV of oligomeric p53 decreases, denoting that cell-to-cell variation is reduced after DNA damage. (*H*) The correlation between each time point postdamage and basal conditions. Lower correlation values mean lower dependency between pre- and post DNA damage. The low correlation of oligomeric p53 by 90 min post damage indicates that all cells converge into a similar state independently of their initial state.

We measured the particle brightness of wild-type p53 and the two mutants at rest and after DNA damage induced by the radiomimetic drug neocarzinostatin (NCS) (Fig. 1*C* and Fig. S2*A*). The increase in brightness following DNA damage results from tetramerization, as only the brightness of wild-type p53 increased (Fig. 1*C*). We used the brightness of the monomeric mutant L344P, ε(mono), to calculate the relative abundance of p53 in each oligomeric state by breaking up the intensity I and the number of molecules N into the specific numbers of p53 monomers M, dimers D, and tetramers T using the following equation:

$$Particle\ \ Brightness := \varepsilon = \frac{<I>}{<N>} = \varepsilon\,(\mathbf{mono}) * \frac{1 + 2\frac{D}{M} + 4\frac{T}{M}}{1 + \frac{D}{M} + \frac{T}{M}}.$$

The FCS brightness analysis was confirmed using photon counting histogram (PCH) analysis (19) on the fluorescence fluctuation data (Fig. S2*B*). We confirmed the reliability of the FCS brightness analysis for quantifying oligomerization by showing that the brightness of fluorescent tandem dimers is double the brightness obtained from monomers in cell lysates using both FCS and PCH analysis (Fig. S2 *C* and *D*). Notably control cells lacking fluorescent reporter showed minimal background and no FCS signal (Fig. S2 *E* and *F*), and photobleaching was found to be minimal (<10%) in our experimental setup (Fig. S2*G*).

Based on the particle brightness obtained from the p53 mutants and the wild-type p53 (Fig. 1*C*), we calculated that at rest the majority of p53 is bound in dimers with 29% unbound monomers and 13% tetramers (Fig. 1 *C* and *D*). Note that the measured mean concentration of p53 in basal conditions (397 nM) was much higher than the dimeric dissociation constant of ~1 nM measured in vitro. However, nearly 30% of p53 molecules are still monomeric, suggesting that additional factors control p53 dimer formation in cells. After DNA damage, the distribution of p53 stoichiometry drastically changed (Fig. 1 *C* and *D*): most p53 was bound in tetramers, with only a small fraction of p53 dimers and monomers. This provides experimental evidence that DNA damage changes the balance of p53 oligomeric state in cells, pushing it toward higher order complexes.

After DNA Damage p53 Tetramerization Precedes Protein Accumulation. To capture the timing of oligomerization and the relationship with total p53 levels, we induced DNA damage and followed both measures in individual cells over time. The total p53 protein (as reported by fluorescence intensity) slowly increases after damage due to stabilization of the protein rather than increased expression (20). p53 oligomerization (reported by the particle brightness) increases more rapidly during the first 90 min, followed by a moderate continuous increase, suggesting that oligomerization precedes stabilization. This order of events is clearly captured when

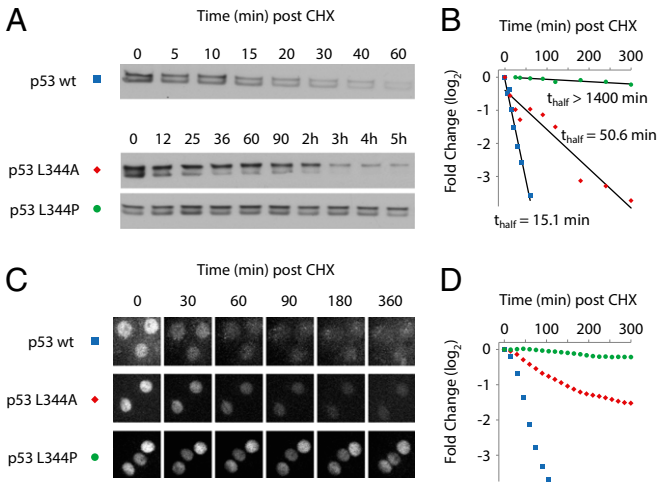

Fig. 2. p53 tetramers are less stable than dimers and monomers. Cells expressing wild-type or mutated p53 were treated with 10 μg/mL cyclohexamide (CHX), and p53 levels were measured using immunoblots (*A* and *B*) and live cell imaging (*C* and *D*). Logarithmic quantification of protein decay was calculated from the blots.

plotting p53 oligomerization against total levels in each cell (Fig. 1*F*).

We observed two additional differences between the dynamics of p53 levels and the oligomeric state of p53 after DNA damage. First, the cell-to-cell variation in p53 total levels remains constant, whereas the variation in oligomeric state decreases with time after damage (Fig. 1*G*). Second, the accumulation in p53 total levels after DNA damage was proportional to the basal level in each cell (Fig. 1*H*), meaning that for the p53 protein levels the initial state of the cells affects its state 3 h after damage. In contrast, by 90 min after DNA damage, the extent of oligomerization was uncorrelated with the oligomeric state in basal conditions (Fig. 1*H*). Taken together this suggests that cells with widely different oligomerization state converge to a common profile of predominantly tetrameric p53 (>90%, Fig. 1*D*) following DNA damage.

Higher Order p53 Oligomers Are Degraded Faster. What can explain the rapid tetramerization of p53 after DNA damaged followed by a delayed accumulation of the p53 protein? One possibility is that tetramerization itself is the mechanism through which the total p53 protein is stabilized. This would imply that the half-life of p53 tetramers should be higher than that of p53 dimers and monomers. We measured the half-life of p53 wild-type and the p53 mutants L344A and L344P in population and single cells (Fig. 2). Surprisingly we found the opposite trend; monomeric p53 showed the longest half-life and wild-type p53 the shortest. Thus, the oligomerization of p53 does not contribute to the stabilization of the protein. The fact that total p53 increases despite the formation of less stable complexes appeared counterintuitive, and we therefore sought to develop a quantitative framework to explore the relationship between oligomerization and stabilization.

The Rapid Surge of p53 Tetramers Requires Active Induction of Tetramerization Together with a Decrease in Degradation. We constructed a mathematical model including three species of p53, corresponding to the three possible oligomeric states (Fig. 3*A* and Tables S1–S3). Monomers of p53, *M*, are produced at a constant rate α and form dimers, *D*, and successively tetramers, *T*. Each species is degraded at a different rate, β_m, β_d, and β_t, respectively. We used the data shown in Figs. 1 and 2 to constrain the parameter values for cells at resting conditions (*Mathematical Modeling and Parameter Search*). We then modeled the effect of DNA damage on the system in several alternative ways and compared each output with the experimental data.

When we modeled DNA damage only as a decrease in p53 degradation by altering the values of βs, our model predicted a faster increase in total p53 levels than in its oligomeric state (Fig. 3*B*). Such behavior was inconsistent with our experimental findings (Figs. 1 and 3*E*). DNA damage modeled only as an induction of p53 tetramerization (by modifying k_ts) led to a decrease in total p53 levels (Fig. 3*C*), which also did not match the experimental data. Only when we modeled DNA damage as a combination of the two effects, decrease in degradation and induction of tetramerization, did the modeled dynamics agree with the measured dynamics (Fig. 3 *D* and *E*). Importantly the fast increase in oligomeric p53 in the model did not depend on the specific choice of parameters (Fig. S3 and *Mathematical*

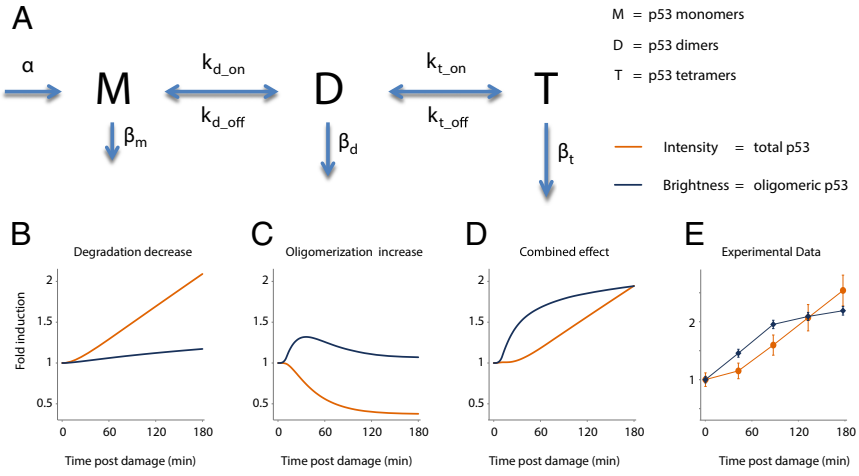

Fig. 3. Mathematical model and simulation of p53 tetramerization and degradation. (*A*) The model includes three species of p53: monomers, M; dimers, D; and tetramers, T. p53 monomers are produced at rate α, and molecules can bind and unbind to form homo-oligomers. Each oligomeric form of p53 can be degraded at rate β_i. (*B–D*) Model simulation for the dynamics of total and oligomeric p53 after DNA damage, modeled in three ways: (*B*) a decrease in p53 degradation, (*C*) an increase in oligomerization, or (*D*) a combination of both effects. (*E*) FCS experimental data showing total and oligomeric p53 (mean and SEM, $n = 18$).

Modeling and Parameter Search). We concluded that both induction of oligomerization and protein stabilization are required for the observed pattern of rapid surge of p53 oligomers after DNA damage followed by increase in total p53 levels.

Assembly of p53 Tetramers Does Not Require Increase in Concentration and Is Sufficient for Activating p53 Transcriptional Targets. Our result supports the existence of a mechanism induced by DNA damage that directly triggers p53 tetramerization independently of its total levels. p53 levels are primarily regulated by degradation, with new molecules constantly being made and degraded. We therefore asked whether tetramerization requires synthesis of new p53 molecules or whether tetramers can be immediately assembled from existing molecules. Our model predicts that inhibition of protein synthesis in the absence of DNA damage should lead to a decrease in both p53 total level and oligomerization level (Fig. 4*A*). After DNA damage is applied, total p53 protein should keep decreasing, whereas the levels of tetrameric p53 should increase. Our experimental FCS measurements matched these predictions; oligomeric p53 increased after DNA damage even when synthesis was inhibited (Fig. 4*B*). We therefore conclude that existing molecules of p53 can be assembled into tetramers.

Is the assembly of p53 tetramers sufficient to induce p53 transcriptional activity? This was previously impossible to determine, as the extent of tetramerization in cells was unknown and tetramer formation was thought to be a direct result of the increase in total p53 concentration. Because we can now separate the increase in total p53 levels from the increase in p53 tetramers (Fig. 4*B*), we can assess the effect of tetramerization on p53 transcriptional activity independent of the increase in its total level. We observed that p53 targets were induced after DNA damage even when p53 levels decreased (Fig. 4*C*). Such induction was not observed when we used a cell line expressing the oligomerization mutant p53 L344A, which forms dimers but not tetramers. These results suggest that tetramerization of p53 is sufficient to activate transcription, without an increase in total p53 protein.

Conclusions

Our results indicate that p53 homo-oligomerization in cells is a highly regulated process. The balance between monomers, dimers, and tetramers is not simply determined by the concentration of p53 molecules. Stress responses, such DNA damage, can trigger p53 tetramerization even when the protein concentration does not increase.

Our study highlights the importance of studying protein homo-oligomerization in cells, where the effects of posttranslational modifications and cofactors modulating oligomerization can be evaluated. Several cofactors have already been shown to regulate p53 oligomerization in vitro. For example, S100 proteins were shown to preferentially bind p53 monomers and inhibit oligomerization (21), and p53 phosphorylation was shown to decrease its tetrameric K_d through binding with 14-3-3σ (11). In addition, p53 binding to specific DNA was suggested to enhance tetramerization (9). Therefore, modifications that increase p53 binding to DNA could have an indirect effect on the oligomerization state of p53. However, even the effects of the known cofactors on the in vitro K_d for p53 tetramerization cannot explain the extent of tetramer concentrations we observed in cells following DNA damage, suggesting the existence of additional unknown regulators of p53 oligomerization. Because our results demonstrate that p53's activity as a transcription factor can be triggered by induction of tetramerization, identification of these unknown factors may point to new targets for modulating p53's function in cancer. The approach we used here should be of general utility in studying the quantitative dynamics and function of oligomerization of transcription factors and other proteins in any cellular system (22).

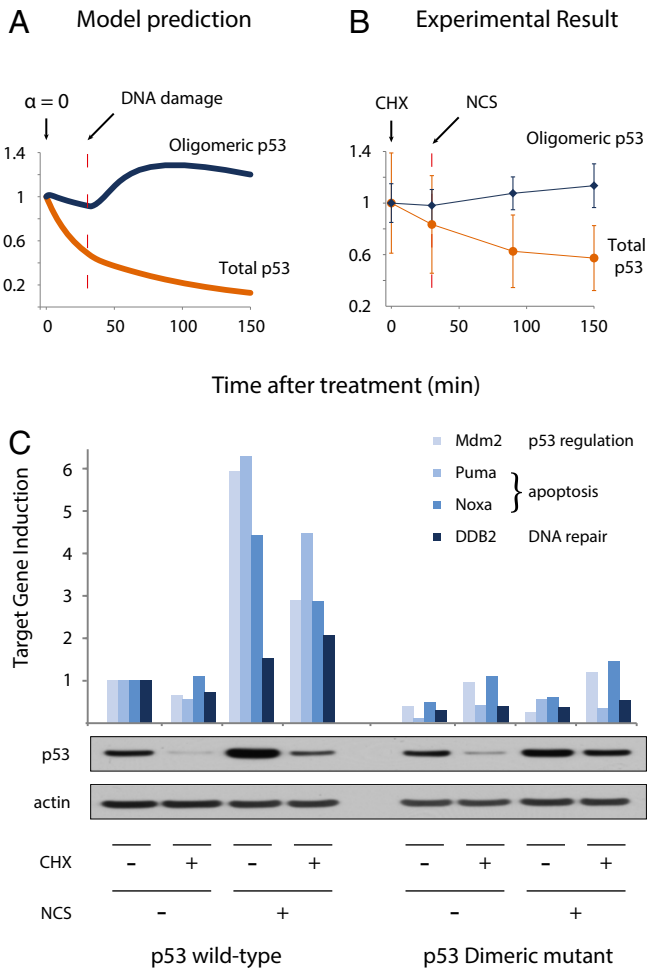

Fig. 4. p53 tetramerization is sufficient for triggering target gene activation without an increase in p53 levels. (*A*) Model simulation of total (orange line) and oligomeric (blue line) p53 after translation inhibition (t = 0), followed by DNA damage. (*B*) Experimental confirmation of the model simulation (mean and SE, $n = 6$). (*C*) p53 transcriptional targets were measured using qPCR in response to DNA damage (NCS) and translation inhibition (CHX) for both wild-type p53 and dimeric mutant p53 L344A. Combination of CHX and NCS leads to an increase in the expression of p53 target genes even when p53 levels are not induced. Induction of p53 target genes is not seen under these conditions for the p53 L344A mutant that can form dimers but not tetramers, suggesting that the induction of p53 targets depends on p53 ability to tetramerize.

Materials and Methods

Cell Line Construction. The cell line MCF7+p53shRNA was kindly provided by the Reuven Agami Group (17), Netherlands Cancer Institute (Amsterdam, The Netherlands). cDNA for p53 was altered by site-directed mutagenesis (QuikChange kit, Stratagene) at residue 344 to obtain oligomerization mutants p53 L344A and p53 L344P, and with seven silent point mutations that allow for mRNA to escape shRNA silencing without altering the amino acid sequence. p53 was expressed under the EF1α promoter and tagged with mCerulean. The vector was introduced in cells via lentiviral infection and stable clonal selection. Lentiviral particles were produced in 293T cells. The fluorescent protein mCerulean has maturation time comparable to Venus (23), which matures in less than 10 min at 37 °C (24).

Cell Culture, DNA Damage, and Cycloheximide Treatment. MCF7+p53shRNA+p53-mCerulean cells were maintained in RPMI supplemented with 100 mL/L FBS, 100 U/mL penicillin, 100 mg/mL streptomycin, and 250 ng/mL fungizone (Gemini Bio-Products) supplemented with selective antibiotics (400 μg/mL G418 and 0.5 μg/mL puromycin). DNA damage was induced by NCS (Sigma) at 400 ng/mL final concentration. Translation inhibition was induced by

cycloheximide (Sigma) at final concentrations of 10 μg/mL for Fig. 2 and 1 μg/mL for Fig. 4. Cells were harvested for protein/RNA extraction at the indicated times after DNA damage and/or translation inhibition.

Western Blot Analysis. Harvested cells were lysed in the presence of protease and phosphatase inhibitors. Total protein levels were quantified using the BCA assay (Pierce). Equal protein amounts were separated by electrophoreses on 4–12% Bis·Tris gradient gels (Invitrogen) and transferred to PVDF membranes by electroblotting. Membranes were blocked with 50 g/L nonfat dried milk, incubated overnight with primary antibody, washed, and incubated with secondary antibody coupled to peroxidase. Protein levels were detected with chemoluminiscence (ECL plus, Amersham). p53 dynamics were quantified by normalizing total p53 levels (DO1, Santa Cruz) to α-actin (Sigma).

Target Gene Expression Dynamics. Total RNA was extracted using the RNeasy protocol (Qiagen). RNA concentration was determined by measuring absorbance at 260 nm. Equal RNA levels were used to generate cDNA using the high-capacity cDNA reverse transcription protocol (Applied Biosystems). Quantitative PCR was performed using reaction mixtures of 8.4 ng total RNA, 100 nM primer, and SYBR Green reagent (Applied Biosystems).

FCS Measurements and Analysis. Two days before microscopy, cells were grown on poly-D-lysinecoated glass-bottom plates (MatTek Corporation). Multiphoton FCS was carried out on a custom-built setup based on a Nikon TE2000 microscope. For mCerulean excitation, a collimated 850 nm IR laser beam (Mai Tai, Ti:Sapphire laser with 80 MHz and 100 fs pulse width, Spectra-Physics) was aligned into Nikon 100× Plan Apochromat oil immersion objective (N.A. = 1.4) with back aperture slightly overfilled, creating a diffraction-limited focal spot. The laser power was controlled below 2 mW to avoid photobleaching of the fusion protein, cellular photodamage, and DNA damage. The collected fluorescence was passed through band-pass filters (HQ485/70m-2p for Cerulean, Chroma Tech) and focused onto a photomultiplier tube (PMT) (H7421, Hamamatsu). The cells were maintained in an aluminum chamber (25) with temperature-controlled water circulation system set to 37 °C. Each autocorrelation curve measured in nucleus was collected for 30 s using Flex02-01D/C correlator (www.correlator.com) and transferred to a personal computer through a high-speed USB port. The PMT dead time is 70 ns, and the correlator dead time is 1.56 ns. The frequency of photon counts was always less than 20 kHz, corresponding to a flow of 2 × 10-5 photon counts per nanosecond, far from the saturation intensity (see sample histogram of photon counts distribution in Fig S2*H*). For average purpose, five FCS curves were recorded at each position in single cell at each time point buffering nonrecurrent kinetics such as the ones caused by extremely slow moving particles. All FCS curves were analyzed by custom-written Matlab code (Mathworks Inc.) using a nonlinear least-squares fitting algorithm from the curve fitting toolbox (2011). The fitting formula for single-component diffusion is adapted from (26):

$$G(t) = \frac{1}{\langle N \rangle}\left(1 + \frac{t}{\tau_D}\right)^{-1}\left(1 + \frac{t}{\omega^2 \tau_D}\right)^{-1/2},$$

where <N> is the average particle number of species in the sampling volume. τ_D is the residence time of species within the sampling volume, with $\tau_D = \omega^2_{xy}/8D$, where D is the diffusion coefficient of the species and $\omega = \omega_z/\omega_{xy}$ is the aspect ratio of the sampling volume. Before the fit analysis, raw FCS autocorrelation curves were denoised by averaging the five curves. Each averaged FCS curve was fitted by the formula above to get the diffusion property, molecule number. The brightness ε was calculated as:

$$\varepsilon = \langle I \rangle * G(0) = \frac{\langle I \rangle}{\langle N \rangle}.$$

Notably, the diffusion coefficient changed minimally over the course of the experiments (Fig. S2*A*), and hence the molecular residence time was constant, indicating that the particle brightness analysis is appropriate in this context (16). Moreover, other proteins that bind p53 could change the diffusion coefficient D; however, because G(0) is independent of D, such binding will not affect the calculated brightness.

Time-Lapse Microscopy. Two days before microscopy, cells were grown on poly-D-lysinecoated glass-bottom plates (MatTek Corporation) in transparent medium supplemented with 50 mL/L FBS, 100 U/mL penicillin, 100 μg/mL streptomycin, and 250 ng/mL fungizone (Gemini Bio-Products). Cells were imaged with a Nikon Eclipse Ti-inverted fluorescence microscope on which the stage was surrounded by an enclosure to maintain constant temperature, CO_2 concentration, and humidity. Images were acquired every 15 min. The CFP filter set was 436/20 nm excitation, 455 nm dichroic beam splitter, and 480/40 nm emission (Chroma). We analyzed images using MetaMorph software (Molecular Devices) and custom-written MATLAB software (Mathworks), which can be downloaded from the Lahav lab webpage (http://lahav.med.harvard.edu).

ACKNOWLEDGMENTS. We thank R. Agami for the MCF7+p53shRNA cell line and B. Ward, E. Natan, P. Cluzel, P. Sorger, A. Loewer, E. Batchelor, A. Ballabeni, and the members of our laboratories for helpful comments and discussion on this work. This research was supported by National Institutes of Health Grants GM083303 and GM077238, and a grant from the Beckman Laser Institute Foundation.

1. Ali MH, Imperiali B (2005) Protein oligomerization: How and why. *Bioorg Med Chem* 13(17):5013–5020.
2. Funnell AP, Crossley M (2012) Homo- and heterodimerization in transcriptional regulation. *Adv Exp Med Biol* 747:105–121.
3. Kitayner M, et al. (2006) Structural basis of DNA recognition by p53 tetramers. *Mol Cell* 22(6):741–753.
4. Imagawa T, Terai T, Yamada Y, Kamada R, Sakaguchi K (2009) Evaluation of transcriptional activity of p53 in individual living mammalian cells. *Anal Biochem* 387(2): 249–256.
5. Kawaguchi T, et al. (2005) The relationship among p53 oligomer formation, structure and transcriptional activity using a comprehensive missense mutation library. *Oncogene* 24(46):6976–6981.
6. Davison TS, Yin P, Nie E, Kay C, Arrowsmith CH (1998) Characterization of the oligomerization defects of two p53 mutants found in families with Li-Fraumeni and Li-Fraumeni-like syndrome. *Oncogene* 17(5):651–656.
7. DiGiammarino EL, et al. (2002) A novel mechanism of tumorigenesis involving pH-dependent destabilization of a mutant p53 tetramer. *Nat Struct Biol* 9(1):12–16.
8. Rajagopalan S, Huang F, Fersht AR (2011) Single-molecule characterization of oligomerization kinetics and equilibria of the tumor suppressor p53. *Nucleic Acids Res* 39(6):2294–2303.
9. Weinberg RL, Veprintsev DB, Fersht AR (2004) Cooperative binding of tetrameric p53 to DNA. *J Mol Biol* 341(5):1145–1159.
10. Sakaguchi K, et al. (1997) Phosphorylation of serine 392 stabilizes the tetramer formation of tumor suppressor protein p53. *Biochemistry* 36(33):10117–10124.
11. Rajagopalan S, Jaulent AM, Wells M, Veprintsev DB, Fersht AR (2008) 14-3-3 activation of DNA binding of p53 by enhancing its association into tetramers. *Nucleic Acids Res* 36(18):5983–5991.
12. Schumacher B, Mondry J, Thiel P, Weyand M, Ottmann C (2010) Structure of the p53 C-terminus bound to 14-3-3: Implications for stabilization of the p53 tetramer. *FEBS Lett* 584(8):1443–1448.
13. Ma L, et al. (2005) A plausible model for the digital response of p53 to DNA damage. *Proc Natl Acad Sci USA* 102(40):14266–14271.
14. Bode AM, Dong Z (2004) Post-translational modification of p53 in tumorigenesis. *Nat Rev Cancer* 4(10):793–805.
15. Weidemann T, Schwille P (2009) Fluorescence correlation spectroscopy in living cells. *Handbook of Single-Molecule Biophysics*, eds Hinterdorfer P, Oijen A (Springer, Dordrecht, The Netherlands), pp 217–241.
16. Macdonald P, Johnson J, Smith E, Chen Y, Mueller JD (2013) Brightness analysis. *Methods Enzymol* 518:71–98.
17. Brummelkamp TR, Bernards R, Agami R (2002) A system for stable expression of short interfering RNAs in mammalian cells. *Science* 296(5567):550–553.
18. Batchelor E, Mock CS, Bhan I, Loewer A, Lahav G (2008) Recurrent initiation: A mechanism for triggering p53 pulses in response to DNA damage. *Mol Cell* 30(3): 277–289.
19. Chen Y, Müller JD, So PT, Gratton E (1999) The photon counting histogram in fluorescence fluctuation spectroscopy. *Biophys J* 77(1):553–567.
20. Brooks CL, Gu W (2011) p53 regulation by ubiquitin. *FEBS Lett* 585(18):2803–2809.
21. Fernandez-Fernandez MR, Veprintsev DB, Fersht AR (2005) Proteins of the S100 family regulate the oligomerization of p53 tumor suppressor. *Proc Natl Acad Sci USA* 102(13):4735–4740.
22. Saunders TE, et al. (2012) Noise reduction in the intracellular pom1p gradient by a dynamic clustering mechanism. *Dev Cell* 22(3):558–572.
23. Kremers GJ, Goedhart J, van Munster EB, Gadella TW, Jr. (2006) Cyan and yellow super fluorescent proteins with improved brightness, protein folding, and FRET Förster radius. *Biochemistry* 45(21):6570–6580.
24. Nagai T, et al. (2002) A variant of yellow fluorescent protein with fast and efficient maturation for cell-biological applications. *Nat Biotechnol* 20(1):87–90.
25. Cramer L, Mitchison TJ (1993) Moving and stationary actin filaments are involved in spreading of postmitotic PtK2 cells. *J Cell Biol* 122(4):833–843.
26. Kim SA, Heinze KG, Schwille P (2007) Fluorescence correlation spectroscopy in living cells. *Nat Methods* 4(11):963–973.